JOURNAL OF MATERIALS SCIENCE 25 (1990) 4607-4613

Thermodynamics for the preparation of SiC–C nano-composites by chemical vapour deposition

Y. WANG, M. SASAKI, T. GOTO, T. HIRAI
Institute for Materials Research, Tohoku University, Sendai 980, Japan

SiC–C nano-composites covering every possible combination of carbon and SiC were prepared by chemical vapour deposition. The specific compositions of the deposits were controlled by changing the Si/C molar ratio in the source gases at deposition temperatures (T_{dep}) of 1673 to 1873 K and total gas pressures (P_{tot}) of 6.7 to 40 kPa using the $SiCl_4$–C_3H_8–H_2 system. The prediction, based on the thermodynamic calculation on composition, morphology and deposition rate, was compared with experimental results. The optimal deposition conditions predicted by the calculations were nearly in agreement with the experimental results.

1. Introduction

In recent years the development of materials which can be utilized under severe temperature conditions, such as experienced in aerospace and nuclear fusion technologies, has been undertaken. One of the approaches in this development is the preparation of "nano-composites" in which a second phase of nanometre size is dispersed in the matrix. Among these, one material receiving considerable attention is the so-called "functionally gradient material" [1, 2], in which the material properties are continuously changed by gradually varying the dispersion-to-matrix ratio from one surface of the material to the other surface. Among these "functionally gradient materials", that consisting of silicon carbide (SiC) and carbon (C) is being examined as a thermal barrier in a space shuttle [2, 3] due to its excellent oxidation resistance and good thermal shock resistance.

Chemical vapour deposition (CVD) is an effective technique in fabricating nano-composites through a co-deposition process using multi-component gas reactions [4, 5]. The main advantage of the CVD technique is the ease with which the composition and microstructure of the deposited materials can be controlled.

There have been several publications [6–10] on the preparation of SiC–C nano-composites by CVD. Yajima and Hirai [6] and Marinković *et al.* [7] prepared carbon (pyrolytic carbon) containing about 5 mol % SiC using $SiCl_4$–C_3H_8 and $SiCl_4$–CH_4, respectively. Yajima and Hirai [8] revealed the size of the dispersed-SiC phase, through TEM observations, to be about 10 to 100 nm.

An improvement in the oxidation resistance has been reported when a small amount of SiC (< 5 mol %) is combined with the carbon matrix by CVD [8]. The CVD SiC–C containing a trace of carbon is shown to be more resistant to abrasion than CVD SiC [9]. Kaae and Gulden [10] prepared SiC–C nano-composite particles containing 55 to 95 mol % C in a fluidized bed furnace using the CH_3SiCl_3–C_3H_8–He system and reported that their Young's modulus and fracture strength increased with increasing SiC content.

In previous reports, the composition (C/(SiC + C)) in the CVD SiC–C was limited to a narrow range, for example, 95 to 100 mol % C in the $SiCl_4$–C_3H_8 [6] and $SiCl_4$–CH_4 [7] systems, 0 to 45 mol % C in the $SiCl_4$–C_3H_8–H_2 system [11], a distinct value of 30 and 60 mol % C in $SiCl_4$–CCl_4–H_2 system [12] and 0 to 72 mol % C in the $(CH_3)_xSiCl_{4-x}$–CH_4 system [13]. Thus, the preparation of SiC–C nano-composite with its composition (C/(SiC + C)) controlled over the entire range has not yet been attempted.

In the present work, as the first step in the development of SiC–C functionally gradient nano-composites, the CVD technique was used to prepare SiC–C nano-composite over all composition ranges. The relationships between deposition conditions and properties of deposited materials were thermodynamically investigated and the optimal deposition conditions are shown.

2. Experimental procedure

2.1. Sample preparation

The experimental set-up is illustrated in Fig. 1. The graphite substrate (40 mm × 12 mm × 2 mm) was heated using an electric current. $SiCl_4$ in liquid form and C_3H_8 and H_2 gases were used as source materials. The deposition temperature (T_{dep}) was selected between 1673 and 1873 K. Previous work [11] has shown that no deposits are obtainable below 1500 K for kinetic reasons and furthermore deposits obtained above 1900 K tend to be porous due to homogenous

TABLE I CVD conditions

Deposition temperature, T_{dep} (K)	1673, 1773, 1873
Total gas pressure, P_{tot} (kPa)	6.7, 13.3, 40
Gas flow rate ($10^{-6}\,m^3\,sec^{-1}$): H_2	0 to 11.7
$SiCl_4$	0 to 3.9
C_3H_8	0.67
Si to C ratio in source gas, $m_{Si/C}$	0 to 1.9
Deposition time, t_{dep} (ksec)	3.6

0022-2461/90 $03.00 + .12 © 1990 Chapman and Hall Ltd.

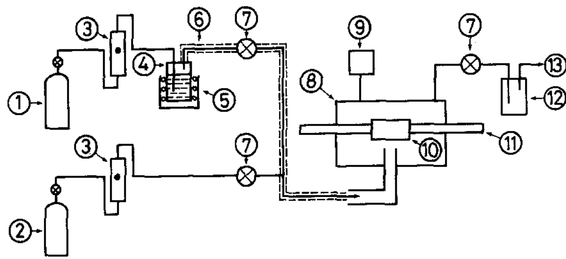

Figure 1 Schematic diagram of deposition apparatus. (1) H_2 gas, (2) C_3H_8 gas, (3) flow meter, (4) $SiCl_4$ reservoir, (5) constant temperature bath, (6) ribbon heater, (7) pressure regulator, (8) reaction chamber, (9) manometer, (10) graphite substrate, (11) electrode, (12) cold trap, (13) rotary pump.

reaction in the gas phase. The total gas pressure (P_{tot}) ranged from 6.7 to 40 kPa. The $SiCl_4$ reservoir was kept at 293 K and its vapour was carried into the furnace by bubbling hydrogen carrier gas. The $SiCl_4$ vapour flow rate was controlled by the hydrogen carrier gas flow rate. The C_3H_8 gas flow rate was kept constant. The molar ratio of silicon to carbon in the source gas ($m_{Si/C}$) ranged from 0 to 1.9. The deposition conditions are shown in Table I.

2.2. Characterization

The free-carbon contents of the deposits were determined by chemical analysis in which powdered samples were burnt in oxygen at 1073 K and the CO_2 gas formed was titrated by coulometry. The structure of the deposits was examined using an X-ray diffractometer (Rigaku: RAD-IIB), and their morphologies were observed by scanning electron microscopy (SEM) (Akashi: Alpha-30 W).

2.3. Thermodynamic calculations

The computer code SOLGASMIX-PV [14] was used to calculate the partial pressures of gas species and the amount of solid species in the equilibrium state. Forty-four gas species and three solid species considered in the present calculations are listed in Table II. These thermodynamic data were taken from JANAF Thermochemical Tables [15]. The theoretical deposition efficiency for carbon or silicon is given by Equation 1

$$\eta_i = \frac{a_i(s)}{a_i(g)} \tag{1}$$

where η_i is the deposition efficiency of atom i, $a_i(s)$ and $a_i(g)$ are the total amount of atom i in the solid and gas phases, respectively.

TABLE II Species considered in $SiCl_4$–C_3H_8–H_2 system

Equilibrium gas species					
SiC	C	Si	H_2	Cl_2	Si_2
Si_3	C_2	C_3	Si_2C	SiC_2	SiH
SiH_4	CH	CH_2	CH_3	CH_4	C_2H
C_2H_2	C_2H_4	$Si(CH_3)_4$	SiCl	$SiCl_2$	$SiCl_3$
$SiCl_4$	CCl	CCl_2	CCl_3	CCl_4	C_2Cl
C_2Cl_4	C_2Cl_6	HCl	CHCl	$CHCl_3$	CH_2Cl_2
CH_3Cl	C_2HCl	SiH_3Cl	SiH_2Cl_2	$SiHCl_3$	$SiCl_3CH_3$
H	Cl				
Equilibrium condensed phases					
Si	SiC	C			

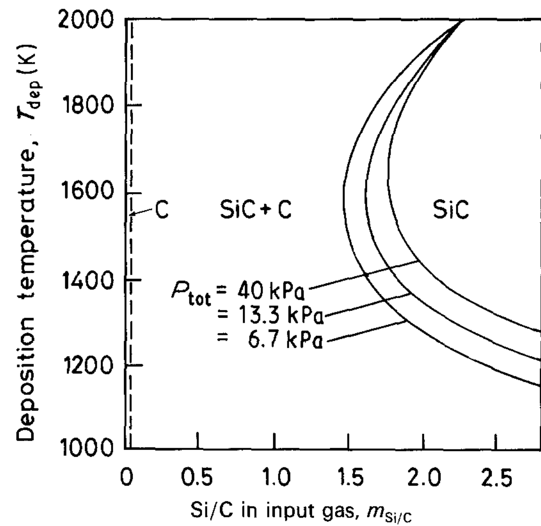

Figure 2 Calculated CVD phase diagram of the $SiCl_4$–C_3H_8–H_2 system.

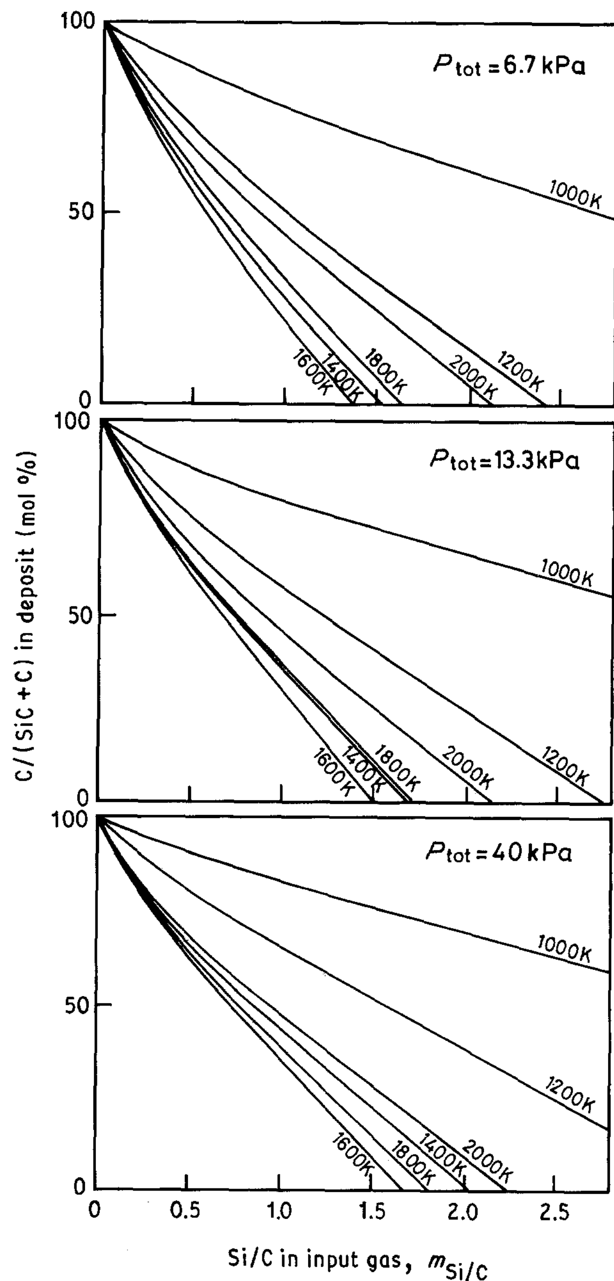

Figure 3 Relationship between calculated compositions and $m_{Si/C}$.

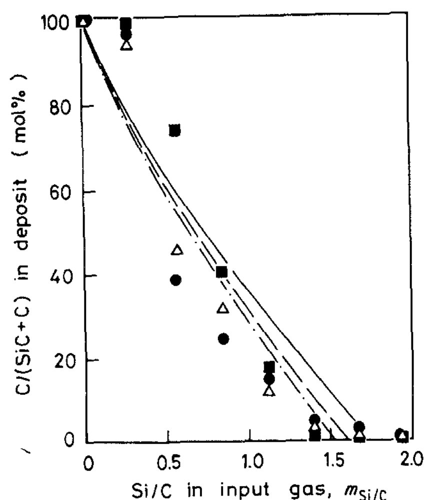

Figure 4 Comparison between calculated (lines) and experimental (points) compositions (T_{dep} = 1673 K). P_{tot} (kPa): (—·—), (●) 6.7; (– – –), (△) 13.3; (——), (■) 40.

3. Results and discussion

3.1. Preparation of CVD SiC–C

Fig. 2 shows the calculated CVD phase diagram of the $SiCl_4$–C_3H_8–H_2 system. The calculation predicts a wide range of deposition conditions for the formation of C + SiC. The SiC single-phase region appears at $m_{Si/C} > 1.5$. A higher $m_{Si/C}$ is required to obtain SiC single-phase as P_{tot} increases. The SiC single-phase region is widest when T_{dep} = 1600 K. No deposition of free silicon is predicted even at $m_{Si/C} > 1$.

Fig. 3 shows the calculated relationship between $m_{Si/C}$ and the C/(SiC + C) composition in the deposits. All compositions between 0% and 100% can be achieved by controlling $m_{Si/C}$ between 0 and 0.28 in the T_{dep} range from 1400 to 2000 K. As clearly seen from Fig. 3, the choice of T_{dep} = 1400 to 1800 K is most suitable because the deviation of composition with T_{dep} is minimal.

The calculated relationships between the composition and $m_{Si/C}$ were compared with the experimental results as shown in Figs 4 to 6. The calculations are in good agreement with the experimental results. The difference between the calculations and experiments decreased with increasing T_{dep}. This result suggests that the formation of SiC–C composites takes place closer to the equilibrium state when T_{dep} is higher.

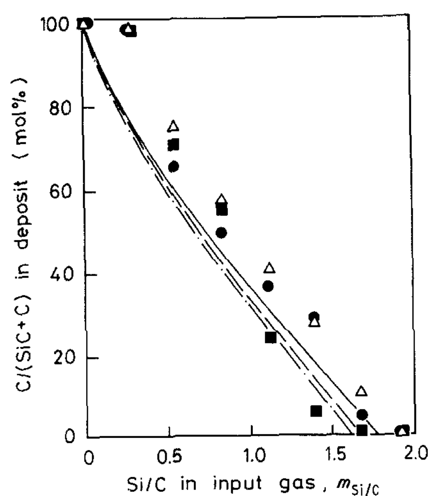

Figure 5 Comparison between calculated (lines) and experimental (points) compositions (T_{dep} = 1773 K). P_{tot}: see Fig. 4.

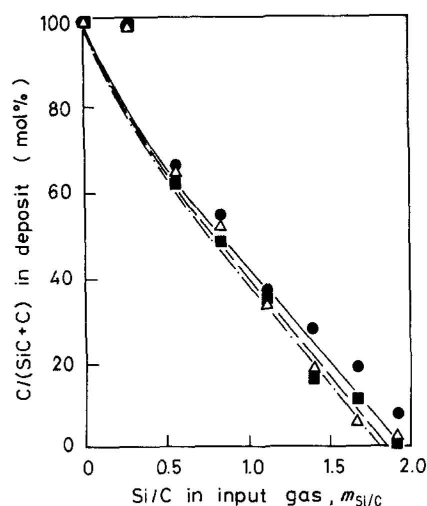

Figure 6 Comparison between calculated (lines) and experimental (points) compositions (T_{dep} = 1873 K). P_{tot}: see Fig. 4.

However, when $m_{Si/C}$ was 0.28, the experimentally obtained carbon contents consistently exceeded the calculated results at every T_{dep} and P_{tot}. Marinković *et al.* [7] and Hirai [16] reported that the presence of $SiCl_4$ vapour in the gas phase can significantly accelerate the deposition of carbon; however, the reason for this was not known. Figs 4 to 6 also show that the single-phase region of SiC shifted to a higher $m_{Si/C}$ with increasing T_{dep}. This tendency is in good agreement with the calculated predictions shown in Fig. 2.

Fig. 7 shows the effect of T_{dep} on the theoretical deposition efficiencies of silicon and carbon atoms. The calculation shows that the theoretical deposition efficiency of the carbon atom is more than 80% in the T_{dep} range from 1000 to 2000 K, and that of the silicon atom reaches a maximum around T_{dep} = 1600 K. All silicon atoms react with carbon atoms to form SiC as shown in Fig. 2.

The relationship between T_{dep} and the equilibrium partial pressure of various gas species is presented in Fig. 8. The most volatile gas species containing silicon atoms changes from $SiCl_4$ to $SiCl_3$ to $SiCl_2$ with increasing T_{dep}. Especially at T_{dep} = 1600 K, the summation of the partial pressure of the gases containing silicon in the gas phase is smaller than at other

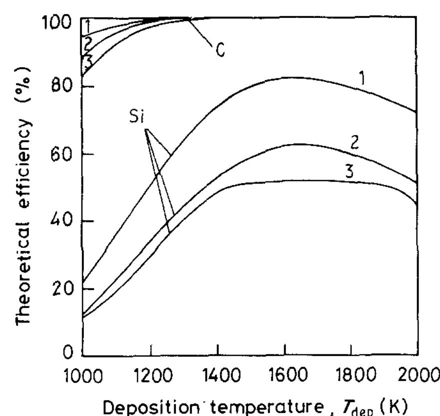

Figure 7 Effect of T_{dep} on theoretical efficiencies for carbon and silicon (P_{tot} = 40 kPa). $m_{Si/C}$: 1, 0.28; 2, 1.1; 3, 1.9.

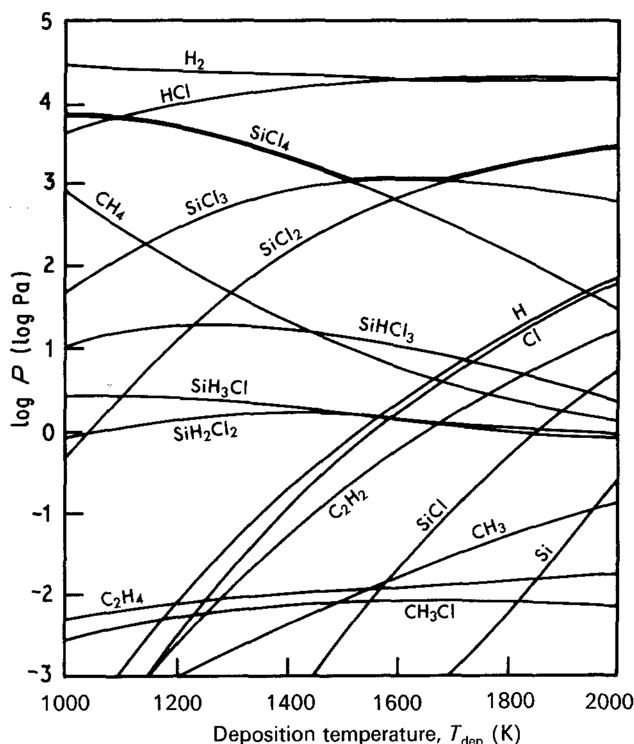

Figure 8 Relationship between T_{dep} and equilibrium partial pressures (P_{tot} = 40 kPa, $m_{Si/C}$ = 1.1).

temperatures, due to the relationship $P_{SiCl_3} > P_{SiCl_4}$ and P_{SiCl_2} indicated by the bold line in Fig. 8. The facts that the theoretical efficiency of silicon is maximum around T_{dep} = 1600 K as shown in Fig. 7 and that T_{dep} = 1600 K is most suitable for controlling the composition of SiC–C as shown in Fig. 3, are the results of the T_{dep} dependency of the equilibrium partial pressure of gases containing silicon.

3.2. Morphology of CVD SiC–C

The morphology of CVD SiC–C prepared by the present work can be divided into two types: "dense-plate" and "porous". Figs 9 and 10 represent typical scanning electron micrographs of the dense-plate and porous deposits, respectively. The deposition conditions (T_{dep} and P_{tot}) and the composition of the deposits determine whether the deposits are dense-plate or porous as indicated by Fig. 11.

The dense-plate region can be extended by decreasing the amount of dispersed phase (i.e. near 0% and 100% on the horizontal axis in Fig. 11), and by increasing P_{tot}. We have previously reported a similar increase in the dense-plate deposition region with increasing P_{tot} in the morphology of CVD SiC [11].

It is generally known that the morphology of CVD materials is affected by the degree of supersaturation of the source gases. The degree of supersaturation is defined by Equation 2 [17].

$$\Sigma_i = \frac{nP^{in}(i)}{\Sigma_j n_j P_j^{eq}(i)} \qquad (2)$$

where Σ_i is the degree of supersaturation of atom i, $P^{in}(i)$ is the partial pressure of the source gas containing atom i, $P_j^{eq}(i)$ is the equilibrium partial pressure of gas species containing atom i (j represents the gas species, i.e. $SiCl_4$, $SiCl_3$, $SiCl_2$, CH_4, C_2H_2 etc.), n and n_j are the number of atoms i contained in the gas species.

Fig. 12 shows the relationship between the equilibrium partial pressure of the gas species and P_{tot} at T_{dep} = 1673 K, $m_{Si/C}$ = 1.1. The partial pressures of $SiCl_4$, C_3H_8 and H_2 in the source gases are also indicated by broken lines in Fig. 12. The degrees of supersaturation of silicon and carbon were calculated from Equation 2 using the values of partial pressure in

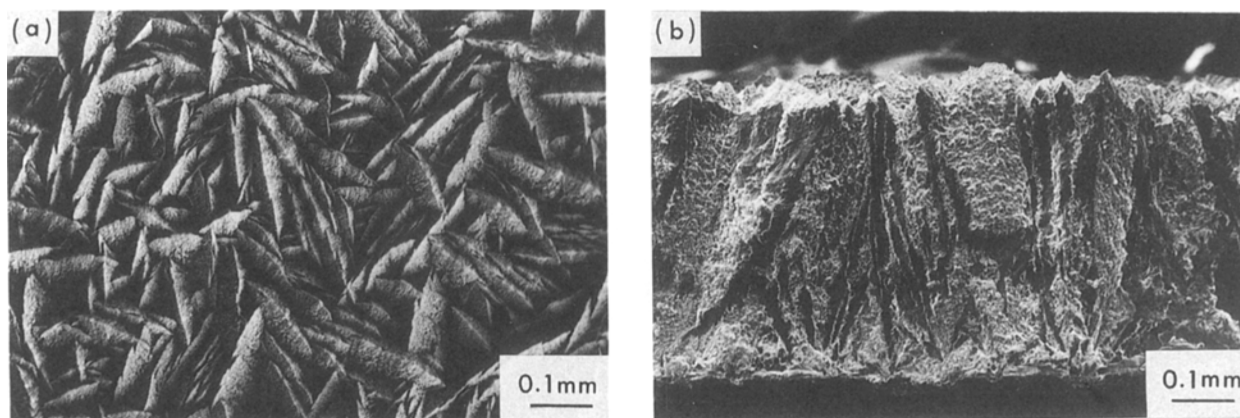

Figure 9 Scanning electron micrographs of the "dense-plate" deposit (SiC–38.9 mol % C) prepared at T_{dep} = 1673 K and P_{tot} = 6.7 kPa: (a) deposited surface, (b) cross-sectional surface.

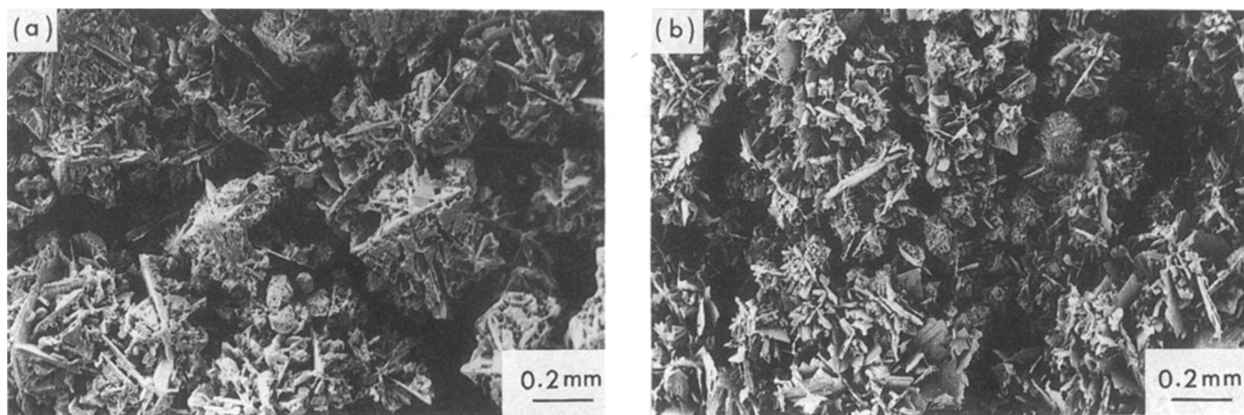

Figure 10 Scanning electron micrographs of the "porous" deposit (SiC–41.1 mol % C) prepared at T_{dep} = 1773 K and P_{tot} = 13.3 kPa: (a) deposited surface, (b) cross-sectional surface.

Fig. 12. Fig. 13 shows the relationship between supersaturation and P_{tot}. Both Σ_{Si} and Σ_C decreased with increasing P_{tot}. The same tendency was reported by Kim *et al.* in a Ti–C system [18].

It is said that particle formation takes places more easily with increasing supersaturation [19] resulting from homogenous reactions in the gas phase. Therefore, the possibility of having greater particle formation in the present work will increase with decreasing P_{tot}, as shown in Fig. 13.

Earlier reports shows that porous deposits of CVD TiB_2 [20] and CVD TiC [21] have been formed depending on the deposition conditions. This porous structure was explained as the effect of particles partially adhering to the substrate and acting as abnormal nucleation-growth sites, and eventually some voids will result in the deposits. In this respect, the morphology of the deposits, as seen in the present work, became porous with decreasing P_{tot} as a consequence of particle formation. Fig. 11 also shows that the morphology of deposits became porous with increasing T_{dep}. This trend agrees well with many results generally known for CVD materials [19].

3.3. Deposition rate of CVD SiC–C

Fig. 14 shows the effect of $m_{Si/C}$ on the growth rate by thickness of CVD SiC–C at T_{dep} = 1673 K. The growth rate varied from 0.05 to 1.3 mm h^{-1} depending on P_{tot} and $m_{Si/C}$. Deposition rates for SiC and carbon by weight were calculated using the growth rates, densities and compositions of CVD SiC–C as shown

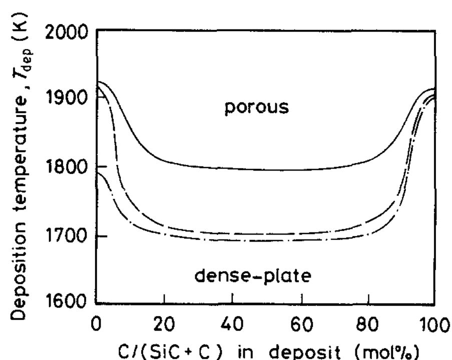

Figure 11 Relationship between morphology, T_{dep} and compositions. P_{tot} (kPa): (——) 40; (— —) 13.3; (—·—) 6.7.

in Fig. 15a. The thermodynamically calculated deposition rates are also shown in Fig. 15b for comparison. The experimentally obtained relationship between the $m_{Si/C}$ and deposition rates (Fig. 15a) is almost in agreement with that of the calculations (Fig. 15b). However, a maximum peak appears in the experimental deposition rate of carbon at $m_{Si/C}$ = 0.28. This peak is a result of the small amount of $SiCl_4$ vapour accelerating the deposition of carbon as mentioned in an earlier section.

Fig. 15a seems to indicate a maximum for the deposition rate of SiC at $m_{Si/C}$ = 1.4. It has been reported that a small amount of free carbon can accelerate the deposition of SiC [11]. The present study confirms this finding.

A comparison of Figs 15a and b indicates that the deposition efficiency is about 20% for both SiC and carbon. The deposition efficiency is defined by the ratio of experimental deposition rate (Fig. 15a) and the calculated rate (Fig. 15b). This value is larger than that reported in many CVD materials whose value is ordinarily of the order of several per cent [22]. The

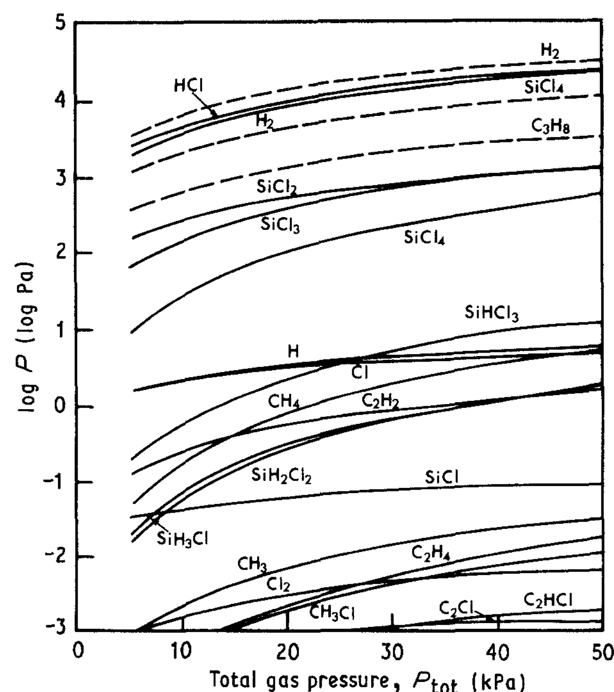

Figure 12 Effect of P_{tot} on equilibrium partial pressures (T_{dep} = 1673 K, $m_{Si/C}$ = 1.1).

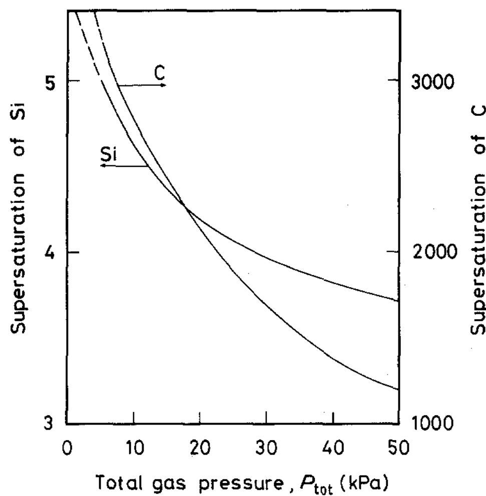

Figure 13 Effect of P_{tot} on supersaturation (T_{dep} = 1673 K, $m_{Si/C}$ = 1.1).

particular type of CVD reactor used in the present work may contribute to the improvement of the deposition efficiency. The cold-wall type used in the present study prevents premature reactions as well as deposition on the reactor-walls.

4. Conclusions

SiC–C nano-composites covering the entire composition range from carbon to SiC were prepared by CVD using the $SiCl_4$–C_3H_8–H_2 system. In order to show the optimum deposition conditions the thermodynamic calculations were compared with the experiments. The following results were obtained.

1. The preparation of SiC–C nano-composites at all compositions is thermodynamically feasible at $m_{Si/C}$ = 0 to 2.8 and T_{dep} = 1400 to 2000 K. The calculation predicted the optimum T_{dep} to be about 1600 K.

2. The composition of SiC–C nano-composites was accomplished over all ranges at T_{dep} = 1673 to 1873 K. The characteristics of the experimentally obtained compositions were in good agreement with the thermodynamic calculations.

3. The morphology of SiC–C nano-composites was of two types: dense-plate and porous. The dense-plate deposits were obtained at lower T_{dep} and higher P_{tot}. The effect of P_{tot} on the morphology was explained by variation in the degree of supersaturation.

4. The relationship between $m_{Si/C}$ and deposition rate was almost in agreement with the calculations. A large deviation from the calculation was observed in carbon-rich composites. The reason for this deviation was explained by the effect of $SiCl_4$ vapour accelerating the deposition of carbon.

5. The deposition efficiencies of SiC and carbon were about 20%. This value is higher than typically reported values. The cold-wall type CVD reactor might have contributed the high efficiency in the present study. A cold-wall type reactor tends to prevent the premature reactions and deposition on the walls.

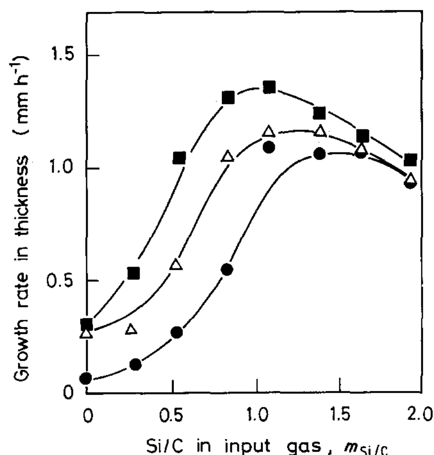

Figure 14 Relationship between growth rate of thickness and $m_{Si/C}$ (T_{dep} = 1673 K). P_{tot} (kPa): (●) 6.7; (△) 13.3; (■) 40.

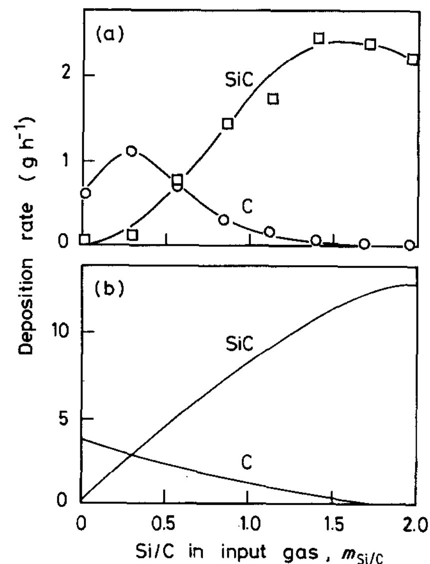

Figure 15 Relationship between deposition rate and $m_{Si/C}$ (T_{dep} = 1673 K, P_{tot} = 40 kPa). (a) Experimental, (b) calculated.

Acknowledgements

The authors thank Messrs G. Makabe and E. Konno for carrying out the free-carbon analysis. This research was supported in part by the Grant-in-Aid for Scientific Research from the Ministry of Education, Science and Culture, under Contract numbers 63 850 149 and 63 750 730.

References

1. T. HIRAI, M. SASAKI and M. NIINO, *J. Soc. Mater. Sci. Jpn* **36** (1987) 1205.
2. M. NIINO, T. HIRAI and R. WATANABE, *J. Jpn Soc. Compos. Mater.* **13** (1987) 257.
3. M. SASAKI *et al., J. Ceram. Soc. Jpn* **97** (1989) 539.
4. T. HIRAI, "Emergent Process Methods for High Technology Ceramics", Materials Science Research Series, Vol. 17, edited by R. F. Davis, H. Palmour III and R. L. Porter (Plenum, New York, 1984) p. 329.
5. T. HIRAI and T. GOTO, in "Tailoring Multiphase and Composite Ceramics", edited by R. E. Tressler, G. L. Messing, C. G. Pantano and R. E. Newnham (Plenum, New York, 1986) p. 165.
6. S. YAJIMA and T. HIRAI, *J. Mater. Sci.* **4** (1969) 416.
7. S. MARINKOVIĆ *et al., Carbon* **8** (1970) 283.
8. S. YAJIMA and T. HIRAI, *J. Mater. Sci.* **4** (1969) 424.
9. M. SASAGAWA *et al.*, in Proceedings of the 95th Meeting of Japan Institute of Metals, Hiroshima, 1984 (Japan Institute of Metals, 1984) p. 149.

10. J. L. KAAE and T. D. GULDEN, *J. Amer. Ceram. Soc.* **54** (1971) 605.
11. T. HIRAI, T. GOTO and T. KAJI, *Yogyo-Kyokai-Shi* **91** (1983) 502.
12. J. J. NICKL and C. V. BRAUNMÜHL, *J. Less-Common Metals* **25** (1971) 303.
13. V. M. BONNKE and E. FITZER, *Ber. Dtsch. Keram. Ges.* **43** (H2) (1966) 180.
14. T. M. BESMANN, ORNL/TM-5775 (April, 1977).
15. "JANAF Thermochemical Tables" 2nd Ed, number NSRDS-NBS-37, edited by D. R. Stull and H. Prophet (US Government Printing Office, Washington, DC, 1971).
16. T. HIRAI, *Bull. Jpn Inst. Metals* **11** (1972) 577.
17. C. S. PARK, J. G. KIM and J. S. CHUN, *J. Electrochem. Soc.* **130** (1983) 1607.
18. D. G. KIM, J. S. YOO and J. S. CHUN, *J. Vac. Sci. Technol.* **A4** (1986) 219.
19. J. M. BLOCHER Jr, *ibid.* **11** (1974) 680.
20. M. MUKAIDA, T. GOTO and T. HIRAI, *J. Mater. Sci.* **25** (1990) 1069.
21. C. JIANG, T. GOTO and T. HIRAI, *ibid.* **25** (1990) 1086.
22. S. MOTOJIMA *et al.*, *ibid.* **21** (1986) 1363.

Received 26 April
and accepted 29 September 1989